International Research Journal of Engineering and Technology (IRJET) e-ISSN: 2395-0056
Volume: 04 Issue: 12 | Dec-2017 www.irjet.net p-ISSN: 2395-0072

Use of Modular Multilevel Cascade Inverter as a Method to Speed-Sensorless Start of an Induction Motor Drive

Ghule Sachin[1], Mushir Uddin[2], Sonje Deepak[3]

[1]*Student & GES, RH SAPAT COE & MS, Nashik*
[2]*Assistant Professor & JES, SND COE & RC, YEOLA*
[3]*Assistant Professor, PG Guide, Dept. of Electrical Engineering,* GES, RH SAPAT COE & MS, Nashik , *Maharashtra, India*

Abstract - *This paper presents theoretical and practical discussions on a experimental speed-sensorless start-up method for an induction motor driven by a modular multilevel cascade inverter based on double-star chopper cells (MMCI-DSCC) from stand- still to middle speed. This motor drive is suitable, particularly for a large-capacity fan- or blower-like load. The load torque is proportional to a square of the motor mechanical speed. The start-up method is characterized by combining capacitor-voltage control with motor-speed control. The motor-speed control with the minimal stator current plays a crucial role in eliminating a speed sensor from the drive system and in dropping an ac-voltage fluctuation occurring across each dc capacitor. Experimental results obtained from the 400-V 15-kW downscaled system with no speed sensor verify that the motor-speed control proposed for the DSCC-based drive system can enhance the start-up torque by a factor of three under the same ac-voltage fluctuation. Several start-up waveforms show stable performance from steady state to middle speed with different load torques.*

Key Words: **Medium-voltage induction motor drives, minimal stator current, modular multilevel cascade inverters, speed- sensorless start-up method.**

1. INTRODUCTION

Attention has been paid to medium-voltage motor drives for energy savings without regenerative brakes [1] – [4]. A modular multilevel cascade inverter based on double- star chopper cells (MMCI-DSCC) has been expected as one of the next-generation medium-voltage multilevel pulse width modulation (PWM) inverters for such motor drives [5]–[14]. For the sake of simplicity, the MMCI-DSCC is referred to as the "DSCC" in this paper [5]. Each leg of the DSCC consists of two positive and negative arms and a center-tapped inductor sitting between the two arms. Each arm consists of multiple bidirectional dc/dc choppers called as "chopper cells." The low- voltage sides of the chopper cells are connected in cascade, while the electrically floating high-voltage sides of chopper cells are equipped with a voltage sensor and a dc capacitor. As the count of cascaded chopper cells per leg increases a synergy effect of lower voltage steps and phase-shifted PWM leads to lower harmonic voltage and current, as well as lower EMI emission,. The power conversion circuit is so flexible of the DSCC in design that any count of cascaded chopper cells is theoretically possible [6].

When a DSCC is applied to an ac motor drive, the DSCC would suffer from ac-voltage fluctuations in the dc-capacitor voltages of each chopper cell in a low-speed range, because as a stator-current frequency gets reduced, the ac-voltage fluctuation gets more serious [7]. Hence, the fluctuation should be attenuated satisfactorily to achieve constant low-speed and start-up performance. Several papers have exclusively discussed start- up methods for DSCC-based induction motor drives [10]–[14]. The authors in [10] proposed a simple start-up method with no speed sensor, in which a DSCC continued to be operated at an appropriate constant frequency, e.g., 30 Hz, to reduce the ac-voltage fluctuation during the start-up. Here, the ac output voltage was adjusted appropriately to produce a required start- up torque. However, an over current may flow not only in the motor but also in the DSCC because slip frequencies in a low speed range get much higher as compare to the rated slip-frequency. This results in producing a reduced motor torque.

For DSCC-driven induction motors other start-up methods from standstill, where each of the motors was equipped with a speed sensor [11]–[14]. A serious ac-voltage fluctuation in a low-speed range can be mitigated by superimposing a circulating current and injecting a common mode voltage on each leg of the DSCC [13]. Usually, it is desirable to eliminate a speed sensor from a motor drive, particularly when a motor drive is introduced to a hostile environment [15], when a new DSCC is applied to an already-existing line-started motor with no speed sensor, or when a long lead cable is required to connect a new DSCC with a new motor.

The aim of this paper is to verify the practicability and effectiveness of a speed-sensorless start-up method for a DSCC- based induction motor drive, in which the motor starts rotating from steady state to middle speed with a ramp change. This motor drive is applicable to a fan- or blower-like load. The load torque is proportional to a square of the

motor mechanical speed [16], and is changing slow enough to be considered as steady-state conditions. The start-up method discussed in this paper is characterized by combining capacitor- voltage control with motor-speed control. The capacitor-voltage control plays a part in regulating the mean dc voltage of each of the dc capacitors [7] and in mitigating the ac voltage appearing across each dc capacitor, which fluctuates at the stator-current frequency [4], [14]. The motor-speed control makes it possible to eliminate a speed sensor from the drive system and to mitigate the ac-voltage fluctuation in all the frequency range.

This motor-speed control relies on an equivalent circuit of an induction motor, which was proposed in [17]. It is somewhat similar in basic idea to conventional "volts-per-hertz" or shortly "*V /f*" and "slip-frequency" control techniques, but different in terms of combining the two control techniques together. The motor-speed control is based on "feedback" control of the stator current, which is the same as that in the slip-frequency control, whereas the commands for the amplitude and frequency of the stator current are based on "feedforward" control in consideration of a speed-versus-load-torque characteristic, as done in the *V /f* control. Therefore, neither motor parameter nor speed sensor is required. Furthermore, the motor-speed control is applicable to any inverter equipped with current sensors at the ac terminals.

Experimental results obtained from a 400-V 15-kW down- scaled system with no speed sensor verify that the motor- speed control with the minimal stator current makes a significant contribution to a reduction of the ac-voltage fluctuations. As a result, the start-up torque is enhanced by a factor of three, without additional stress on arm currents and dc-capacitor voltages. Several start-up waveforms show steady performance from steady state to middle speed with different load torques.

1.1 Circuit Configuration and Capacitor-Voltage Control of the DSCC

Fig. 1(a) shows the main circuit configuration of the DSCC discussed in this paper. As shown in Fig. 1(b) Each leg consists of eight cascaded bidirectional chopper cells and , as shown in Fig. 1(c) a center- tapped inductor per phase. The center tap of each inductor is connected directly to each of the stator terminals of an induction motor, where i_u is the *u*-phase stator current. The center-tapped inductor is more cost effective than two non coupled inductors per leg, because the center tapped inductor presents inductance L_Z only to the circulating current i_Z and no inductance to the stator current i_u [7]. It brings significant reductions in weight, size, and cost of the magnetic core. These advantages in the center-tapped inductor are mostly welcomed, particularly applications to motor drives, in which no ac inductors are required between the inverter and the motor. In Fig. 1, instantaneous currents i_{Pu} and i_{Nu} are the *u*- phase positive- and negative-arm currents, respectively, and i_{Zu} is the *u*-phase circulating current defined as follows[7]:

$$i_{Zu} \triangleq \frac{1}{2}(i_{Pu} + i_{Nu}) \qquad (1)$$

[1]Detailed discussions on the center-tapped inductor in terms of power loss and size are beyond the scope of this paper.

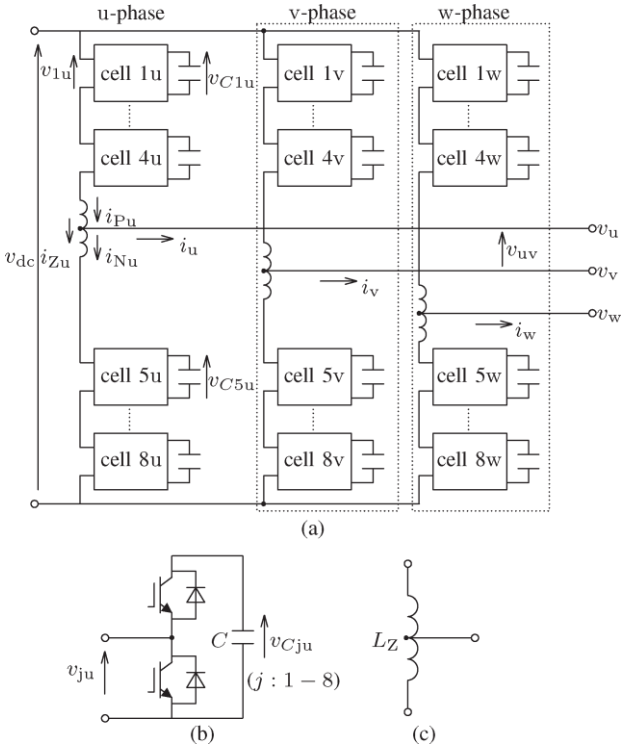

Fig 1: Circuit configuration for an MMCI-DSCC. (a) Power circuit. (b) Chopper cell. (c) Center-tapped inductor.

Note that i_{Zu} includes dc and ac components to be used for the capacitor-voltage control. The dc component flows from the common dc link to each leg, while the ac component circulates among the three legs. The individual ac components included in the three-phase circulating currents $\tilde{i}_{Zu}$, $\tilde{i}_{Zv}$, and $\tilde{i}_{Zw}$ cancel each other out, so that no ac component appears in either motor current or dc-link current [14].

The arm currents i_{Pu} and i_{Nu} can be expressed as linear functions of two independent variables i_u and i_{Zu} as follows [7]:

$$i_{Pu} = \frac{i_u}{2} + i_{Zu} \qquad (2)$$

$$i_{Nu} = \frac{i_u}{2} + i_{Zu} \quad (3)$$

The dc-capacitor voltage in each chopper cell consists of ac and dc components causing an ac-voltage fluctuation. When neither common-mode voltage nor ac circulating current is superimposed, the peak-to-peak ac-voltage fluctuation Δv_{Cju} is approximated as follows [10]:

$$i_{Zu} \triangleq \frac{1}{2}(i_{Pu} + i_{Nu}) \quad (4)$$

Where I_1 is the rms value of the stator current, f is the frequency of the stator current, and C is the capacitance value of each dc capacitor. According to (4), Δv_{Cju} is inversely proportional to f and proportional to I_1. Hence, Δv_{Cju} increases as the stator-current frequency decreases. Increasing the ac-voltage fluctuation is undesirable due to the following reasons [14].

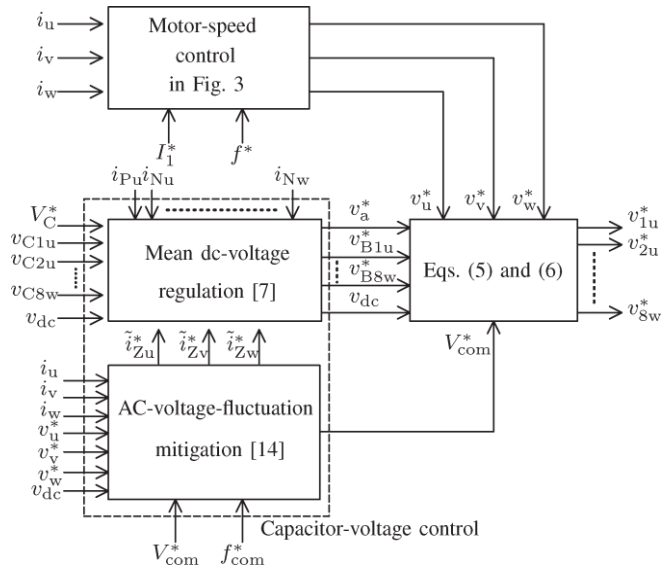

Fig 2: Overall control block diagram for the start-up method

- It affects the voltage rating of insulated-gate bipolar transistors.
- It causes over modulation to each chopper cell.
- It makes the system unstable because the ac-voltage fluctuation can be considered as a disturbance to the control system.

Therefore, the ac-voltage fluctuation should be mitigated to an acceptable level.

1.2 CAPACITOR-VOLTAGE CONTROL

Fig. 2 shows the overall control block diagram of the startup method. The 24 dc-capacitor voltages v_{Cjuvw}, the dc-link voltage v_{dc}, and the six arm currents i_{Nuvw} and i_{Puvw} are detected, and they are input signals for the block diagram. Note that the three stator currents i_{uvw} are calculated from the detected arm currents. This paper employs two kinds of existing capacitor-voltage control techniques for regulating the mean dc voltage of each dc capacitor and for mitigating the ac-voltage fluctuation at the stator-current frequency.

The mean dc-voltage regulation can be achieved by using the "arm" balancing control applied to the six arms and the "individual" balancing control applied to the one arm at the same time [7]. The ac-voltage fluctuation can be mitigated by the sophisticated control discussed in [13]. This control interacts the common-mode voltage v_{com}, which is injected to three center-tap terminals of the DSCC with the ac components of the three circulating currents $\tilde{i}_{Zuvw}$. This can mitigate the ac- voltage fluctuation at the stator-current frequency, thus leading to start up from standstill. As a result, the remaining ac-voltage fluctuations are independent of the time-varying frequencies of the stator current, but dependent on a fixed frequency of the injected common-mode voltage (50 Hz in this experiment). The circulating-current feedback control included in the mean dc-voltage regulation block yields a command voltage of v_a^*.

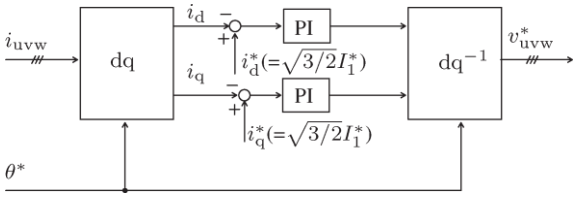

Fig 3: Block diagram for the motor-speed control based on a feedback control of the stator current.

Finally, command u-phase voltages for each chopper cell, i.e., $v_j{}^*{}_u$, are given as follows [14]:

$$v_{ju}^* = v_a^* + v_{Bju}^* + \frac{v_a^* + v_{com}^*}{4} + \frac{v_{dc}}{8}(j = 1 - 4) \quad (5)$$

$$v_{ju}^* = v_a^* + v_{Bju}^* + \frac{v_a^* + v_{com}^*}{4} + \frac{v_{dc}}{8}(j = 5 - 8) \quad (6)$$

Here, v_a^* and $v_{B\,ju}^*$ are used to regulate the mean dc voltage, v_u^* is the command motor voltage given by Fig. 3 described in the later section, v_{com}^* is the command common-mode voltage, and V_{dc} is the dc-link voltage used as feed forward control. The command rms value of the common-mode voltage v_{com}^* should be set as high as possible to reduce the amplitude of each ac circulating current, because it is inversely proportional to V_{com} [14]. Moreover, there is no relationship between common-mode voltage and power rating of the motor.

This paper switches over the two capacitor-voltage control techniques according to the stator-current frequency as follows.

- In a low-speed range of f 12 Hz, the rms value of the common-mode voltage V_{com} and the ac circulating currents $\tilde{i}_{Zuvw}$ are controlled actively to mitigate the ac- voltage fluctuation of each dc-capacitor voltage [14].
- When f 20Hz, neither V_{com} nor $\tilde{i}_{Zuvw}$ is superimposed.

During a frequency range of 12 ≤ f ≤ 20 Hz, V^*_{com}, and i^*_{Zuvw} decrease linearly in their amplitude. Note that the dc circulating current is used to regulate the mean dc voltage of each dc capacitor through all frequency range [10].

1.3. MOTOR-SPEED CONTROL

This section describes a motor-speed control forming a feed- back loop of three-phase stator currents for achieving a stable start-up of an induction motor. First, the motor-speed control is discussed in terms of a form and function. Second, it is compared with conventional motor-speed control techniques, i.e., "volts-per-hertz" and "slip-frequency" control techniques.

A. Control Principles

The motor-speed control forms a feedback loop of three-phase stator currents to realize a stable start-up from standstill. This requires the current sensors attached to the ac terminals. The stator current in one phase is calculated by the corresponding arm currents detected. Therefore, no additional current sensor is required.

Fig. 3 shows the block diagram for the motor-speed control. The three-phase stator currents are transformed into dc quantities by using the d q transformation to enhance current controllability. In Fig. 3, θ^* is the phase information used for the d q transformation, whereas i^*_d and i^*_q are the command currents given by

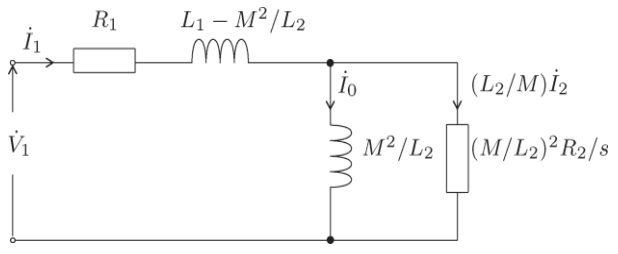

Fig 4: Per-phase equivalent circuit based on the total linkage flux of the secondary windings [17].

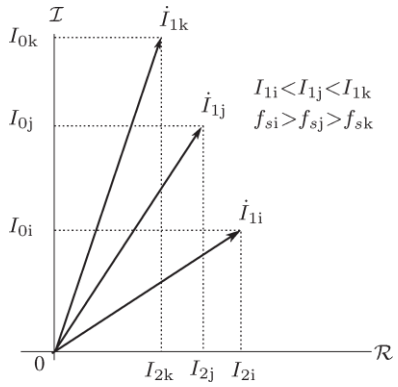

Fig 5: Phasor diagram for the stator currents with different amplitudes but the same torque.

$$i_d^* = i_q^* = \sqrt{\frac{3}{2}} i_1^* \qquad (7)$$

Where I_1^* is the command for the stator rms current. Note that I_1^* and f^* are given not by feedback control, but by feed forward control, as described later.

Fig. 4 shows a per-phase equivalent circuit of an induction motor based on the total linkage flux of the secondary windings [17]. Although this circuit is valid only under steady-state conditions, it is applicable to a fan- or blower-like load, in which the motor mechanical speed is adjusted slow enough to be considered as the steady-state condition. Here, $\dot{I}0$ is the phasor magnetizing current, $\dot{I}1$ is the phasor stator current and $\dot{I}2$ is the phasor torque current. Note that $\dot{I}0$ and $\dot{I}2$ are orthogonal to each other in steady-state conditions. The rms value of $\dot{I}1, I_1$ is given in Fig. 4 as follows:

$$I_1 = \sqrt{I_0^2 + (\frac{L_2}{M} I_2)^2} \qquad (8)$$

The motor torque T_M is expressed by using I_0 and I_2 that are the rms values of $\dot{I}0$ and $\dot{I}2$, respectively, as follows [17]:

$$T_M = 3PMI_0I_2 \qquad (9)$$

Where, P is the pole-pair number.

Fig. 5 shows a phasor diagram for three different phasor stator currents $\dot{I}1i, \dot{I}1j$, and $\dot{I}1k$ but with producing the same torque, in which a relation of $I_{1i} < I_{1j} < I_{1k}$ holds. The imaginary flame corresponds to the magnetizing current I0, and the real flame corresponds to the torque current I_2. It is obvious in (9) and Fig. 5 that the motor torque T_M is proportional to the area of the triangle surrounded by $\dot{I}1$, I_2, and I_0.

The motor-speed control has no capability to control the magnetizing current and the torque current independently. However, when the phasor stator current changes from $\dot{I}_{1i}$ to $\dot{I}_{1j}$, the torque current decreases from I_{2i} to I_{2j} and the magnetizing current increases from I_{0i} to I_{0j}, respectively, to keep the area of triangle constant. In other words both I_0 & I_2 would change each of the amplitude automatically when I_1 changes. The slip frequency f_s is described by using I_2 and I_0 as follows [17]:

$$f_8 = \frac{R_2}{2\pi M}\frac{I_2}{I_0} \qquad (10)$$

A relation of $f_{si} > f_{sj} > f_{sk}$ exists in Fig. 5, which are the slip frequencies at different operating points. The slip frequency has no freedom when T_M and I_1 are given.

B. Comparisons of Three Motor-Speed Control Techniques

Table 1 summarizes comparisons among the three motor- speed control techniques, with a focus on similarity and difference.

The "volts-per-hertz" control or shortly "V/f" control has two independent variables V_1 and f, in which V_1 is the stator voltage & f is the stator frequency. On the other hand the two dependent variables the slip frequency f_s and are the stator current I_1. The V/f control is a straightforward speed control requiring no speed sensor, which is based on feed forward control of f and V_1. However, both DSCC and motor may suffer from an over current during the start-up or when a rapid change in torque occurs.

The slip-frequency control has two independent variables I_1 and f_s, and the two dependent variables are V_1 and f. Here, the commands for f_s and I_1 are determined by a feedback loop of the motor mechanical speed, thus requiring a speed sensor attached to the motor shaft. The slip-frequency control can provide a faster torque response than the V/f control because of the existence of a feedback control for the motor mechanical speed.

The motor-speed control proposed for the DSCC-based induction motor drive has two independent variables f *and* I_1, and the two dependent variables are f_s and V_1. Unlike the slip- frequency control, the motor-speed control requires no speed sensor because the commands for I_1 and f, i.e., I_1^* and f^*, are given not by feedback control, but by feed forward control, as done in the V/f control. This implies that the motor- speed control proposed in this paper is inferior to the slip- frequency control, in terms of torque controllability. However, it is applicable to a fan or blower like load, where the load torque is changing relatively slow and predictable [16]. Moreover, no over current occurs during the start-up, or when a rapid change in torque occurs, because of the existence of a feedback control loop of the stator current.

Table -1: COMPARISONS AMONG EXISTING VOLTS-PER-HERTZ AND SLIP-FREQUENCY CONTROL TECHNIQUES AND THE PROPOSED MOTOR-SPEED CONTROL TECHNIQUE

	Volts-per-Hertz control	Slip frequency control	Proposed motor-speed control
Independent variables	V_1 and f	I_1 and f_s	I_1 and f
Dependent variables	I_1 and f_s	V_1 and f	V_1 and f_s
Voltage control	Feedforward	-	-
Current control	-	Feedback	Feedback
Speed sensor	No	Yes	No

An energy saving during a start-up does not make a significant contribution to total energy saving performance from a practical point of view because the motor power in a low speed range is very less in applications such as fan or blower like loads. This means that a comparison of the three methods, in terms of energy saving performance during a start-up, does not make sense when fan or blowers like loads are considered. Moreover, current stresses of the conventional motor-speed control techniques, the V/f and slip-frequency control, and the proposed motor-speed control technique are the same, at least, in a steady-state condition when a magnetizing current is set to the same value in all speed range.

1.4 COMMAND STATOR CURRENTS

This section describes how to determine the command of the stator rms current I^* and the stator-current frequency f^*. The following two methods can be used to determine I_1^* and f^*:

1. determination from the equivalent circuit shown in Fig. 4;
2. Determination from experiments.

A. Design Considerations

The following practical limitations should be imposed on I_1^*.

1. I_1^* should take the smallest current to produce a desired motor torque T_M.

2. The maximum value of each arm current is lower than

The first condition should be met because as I_1^* gets larger, Δv_{Cju} gets higher, as predicted from (4). In other words, minimizing I_1^* enables minimization of ΔvCju. The second limitation should be met because an increase in the arm currents

Brings additional loss to a DSCC and makes the center-tapped inductors larger and heavier. Note that such an increase in the arm currents occurs particularly in low-speed operation, where a large amount of ac circulating current is superimposed on each arm current. The ac circulating current superimposed Results in mitigating the ac-voltage fluctuation appearing across the dc capacitor of each chopper cell. Hence, I_1^* should be reduced because the ac component of the arm current is proportional to I_1^* [14].

B. Determination From the Equivalent Circuit Shown in Fig. 4

When a speed-versus-load-torque characteristic is known, the equivalent circuit shown in Fig. 4 can be used to determine I_1^* and f^*, along with the motor parameters including moment of load inertia. The motor torque should satisfy the following equation during the start-up:

$$T_M - T_L > (J_M + J_L)\frac{d\omega_{rm}}{dt} \qquad (11)$$

Where T_L is the load torque, J_M is the moment of inertia of the motor, J_L is that of the load, and ω_{rm} is the mechanical-angular velocity. The right-hand term on (11) corresponds to an acceleration torque for the start up.

For making analysis simple and easy, the following reason- able approximations are made.

- The stator-current frequency f agrees well with its command f^* (i.e., $f = f^*$).
- The slip frequency f_s is much smaller than f (i.e $f_s \ll f$).

The moment of inertia of the load J_L is much larger than that of the motor J_M (i.e., $J_M \ll J_L$).

These three assumptions are applicable to fan or blower like loads for the following reasons. The first assumption is valid because the motor mechanical speed, or the motor frequency, is adjusted slowly, e.g., spending a few or several minutes to complete its start-up procedure. The second assumption is reasonable for an induction motor. The third assumption is valid because J_L is typically 50–100 times larger than J_M[10].

Finally, (11) is simplified as follows:

$$T_M - T_L > J_L \frac{2\pi}{P}\frac{df^*}{dt} \qquad (12)$$

the amplitude of the rated stator current.

Where $\omega_{rm} = 2\pi f^*/P$. Equation (12) means that the acceleration torque is proportional to the slope of change in f^*. This suggests that the minimum torque required for the motor start-up is $T_M = T_L$, when the term on the right-hand side in (12) is small enough to be negligible. In other words, the slope of f^* should be set to be as small as possible to reduce the acceleration torque.

The motor torque T_M in Fig. 5 is proportional to the area surrounded by I'_1, I_2, and I_0. The stator rms current required to produce a motor torque gets the smallest when the following relation is met:

$$I_0 = \frac{L_2}{M0} I_2 \qquad (13)$$

Substituting (13) into (9) yields

$$I_0 = \sqrt{\frac{T_M}{3PL_2}}\, I_2 \qquad (14)$$

Finally, I_1 is obtained by substituting (14) into (8) as follows:

$$I_1 = \sqrt{\frac{2L_2T_M}{3PM^2}} \qquad (15)$$

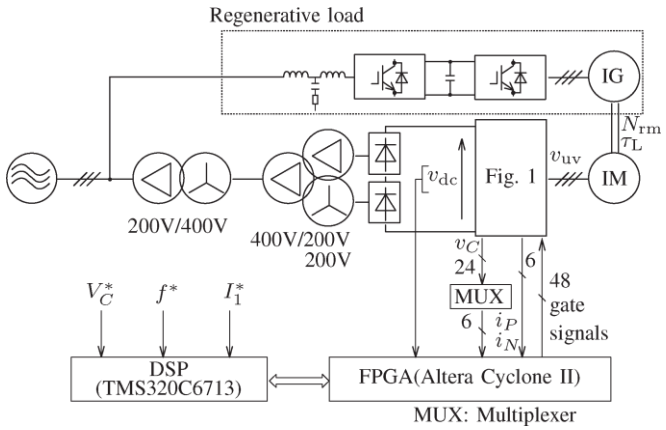

Fig 6: 400-V 15-kW downscaled system used in the experiments

C. Determination From Experiments

When a speed-versus-load-torque characteristic is unknown, the current command I_1^* should be determined experimentally as follows. The initial value of I_1^* is set to zero. Then the motor starts rotating as, I_1^* is being increased gradually.

This method is similar to a traditional V/f control, in terms of no use of motor parameters.

It is difficult to apply the motor-speed control to an application where a rapid or irregular change in load torque

May happen the reason is that $I_1^*$and $f^*$are given by feed forward control with no capability of handling a rapid or irregular change in torque. However, the motor-speed control is applicable to a fan- or blower-like load, where the motor mechanical speed is adjusted slowly, and the load torque of which is proportional to a square of the motor mechanical speed [16]. In this case, I_1 should be given so that it is proportional to the command motor mechanical speed, as predicted from (15). In addition, I_1 is proportional to the stator-current frequency f because the slip frequency f_s is typically negligible compared to the stator-current frequency ($f_s f$).

Finally, experimental adjustment of the slope of I_1/f ($=I_1^*/f^*$) is required to achieve the stable start-up so called "torque boost" function at low speeds, which is used in the V/f control [18], is applicable to the motor-speed control.

2. EXPERIMENT

2.1 Experimental System Configuration

Fig. 6 shows the system configuration of the 400-V 15-kW own scaled system. Table 2 summarizes the circuit parameters used in the experiments. Table 3 summarizes the specifications of the 380-V 15-kW induction motor tested. Here, a three phase 12-pulse diode rectifier, consisting of a three-winding transformer with a Δ–Δ–Y connection and two three-phase six-pulse diode rectifiers, is used as the front end. When the supply voltage matches the motor voltage, a transformer less medium-voltage motor drive can be achieved by replacing the 12-pulse diode rectifier with a six-pulse diode rectifier. Neither electrolytic capacitor nor film capacitor is connected to the common dc link [20].

The ac output terminals of the DSCC are directly connected to the induction motor rated at 380 V and 15kW. The regenerative load in Fig. 6 consists of an induction generator rated at 190 V and 15 kW and two identical PWM converters connected back to back. The field oriented control is applied to the induction generator, which enables an arbitrary instantaneous torque τ_L to be loaded on the induction motor.

Table-2: Circuit Parameters used in the Experiments

Rated active power		15kW
Rated line-to line rms voltage	Vs	400V
Rated dc-link voltage	Vdc	570V
Center-tapped inductor	Lz	4.0 mH
		(12%)
DC capacitor of chopper cell	C	3.3 mF
DC- capacitor voltage	Vc	140V
Unit capacitance constant	H	52 MS[19]
Cell count per leg	N	8
Triangular-wave-carrier freq.	Fc	2 kHz
Equivalent carrier frequency	N fc	16 kHz

*The value in 0 is on a 400V, 15KW and 50-Hz base

Table-3: Motor Parameters used in the Experiments

Rated output power		15 kW
Rated frequency		50 Hz
Rated line-to-line rms voltage	V	380V
Rated mechanical speed	Nrm	1460min^{-1}
Rated stator rms current	I1	32 A
Rated magnetizing current	I0	184 A
Pole-pair number	P	2
Moment of motor inertia	J_M	0.1 kg*m^2
Moment of load inertia	J_L	0.1 kg*m^2

The field-programmable gate array (FPGA) block shown in Fig. 6 detects the 24 dc-capacitor voltages V_{Cjuvw}, the dc-link voltage V_{dc}, and the six positive- and negative-arm currents i_{Puvw} and i_{Nuvw}. These are input signals to the A/D converters in the FPGA. Here, four multiplexers are used to reduce the number of the analog signals from 24 to six. The digital signal processor (DSP, Texas Instrument TMS320C6713) takes in the digital signals from the A/D converters and produces the command voltage of each chopper cell. The FPGA block produces 48-bit (= 2 24) gate signals receiving from the DSP block in total. Note that the motor mechanical speed N_{rm} is obtained from a tacho generator attached to the motor shaft, which is not for control but for measurement.

An over current protection for each chopper cell has been implemented, in which the DSCC is disconnected from the ac mains when amplitude of either of the arm currents reaches 45 A. The command dc-capacitor voltage was set to V_C^* =140 V. A square-wave common-mode voltage and square-wave circulating currents were used to mitigate the ac-voltage fluctuation of each dc capacitor, in which the rms value of the common-mode voltage V_{com} and its frequency f_{com} were set to V_{com} = 180 V and f_{com} = 50 Hz, respectively, for the following reasons.

- The command common-mode voltage V_{com}^* was set to

make the modulation index of the DSCC be around unity [14].

- The command frequency f^*_{com} was set to be less than one-tenth of the carrier frequency of f_C (i.e., $f_{com}f_C/10$ = 200 Hz) to achieve good controllability of the ac circulating current [14].

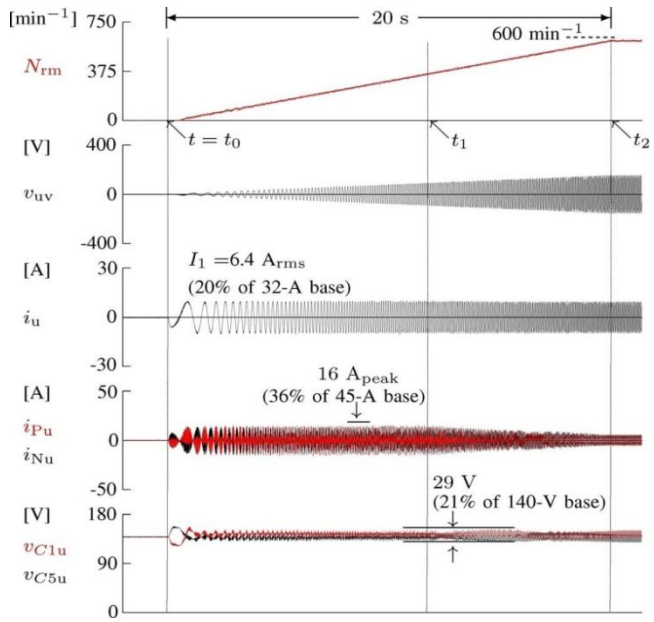

Fig 7: Experimental start-up waveforms when I_1^*= 6.4 A (20%) and TL = 0%, where I0 = 6.4 A (35%).

The command for the stator rms current I_1^* in the motor-speed control was determined by experiments.

2.2 Start-Up Performance

Figs. 7–11 show experimental start-up performance with different load torques. The harmonic voltages included in the line-to-line voltage v_{uv} were eliminated by using a low-pass filter with a cutoff frequency of 400 Hz. The command for the stator-current frequency f^* was being changed from zero to

20 Hz under a ramp change rate of 1 Hz/s. The acceleration torque is obtained in Table III and (12) as 0.7% of the rated torque, which is small enough to be negligible. Hence, a relation of T_M T_L holds.

Fig. 7 shows the experimental start-up performance with no load torque. Here, I_1^* was set to 6.4 A, which is 20% of the rated stator rms current of 32 A. The motor mechanical speed was increasing from zero to a synchronous speed of 600 min^{-1} without overshoot or undershoots. The rms value of the stator current i_u was regulated at 6.4 A, without any steady-state error, by applying the feedback control shown in Fig. 3. A relation of I_1 = I_0 exists in Fig. 5 because both load and acceleration torque were zero from a practical point of view. The amplitude of v_{uv} was increasing linearly as N_{rm} was increasing because I_0 (= I_1) was regulated at almost the constant value.

A square-wave common-mode voltage with V_{com} = 180 V and f_{com} = 50 Hz and square-wave circulating currents were superimposed during $t_0 \leq t \leq t_1$ to mitigate the ac-voltage fluctuation of each dc-capacitor voltage. During t1 ≤t ≤$t2$, the amplitude of the common-mode voltage and the ac circulating currents were decreasing linearly, and they were set to zero when $t_2 \leq t$. As a result, the amplitude of i_{Pu} and i_{Nu} during $t_0 \leq t \leq t_1$ were larger than those during t2 ≤ t. However, the maximum value of the arm currents was smaller than the amplitude of the rated stator current of 45A($= \sqrt{2} \times 32A$)

The maximum amplitude of the arm currents was 16 A, which is 36% of 45 A. The mean dc voltages of $vC1u$ and $vC5u$ were regulated at the command value of 140 V. The peak-to-peak ac voltage fluctuation of $vC1u$ and $vC5u$ was 29 V, which is 21% of 140 V. Fig. 8 shows the experimental start-up performance with TL = 20%. Here, I_1^* was set to 10 A (31%), which is the minimal value to produce a motor torque of 20%. The magnetizing current $I0$ calculated from (8) and (13) reached 7.0A (= 10 A/$\sqrt{2}$), which is 38% of the rated magnetizing current of 18.4 A. The motor mechanical speed was increasing up to 591 min−1, where the slip frequency was fs = 0.30 Hz. The maximum amplitude of the arm currents was 23 A, which is 51% of 45 A.

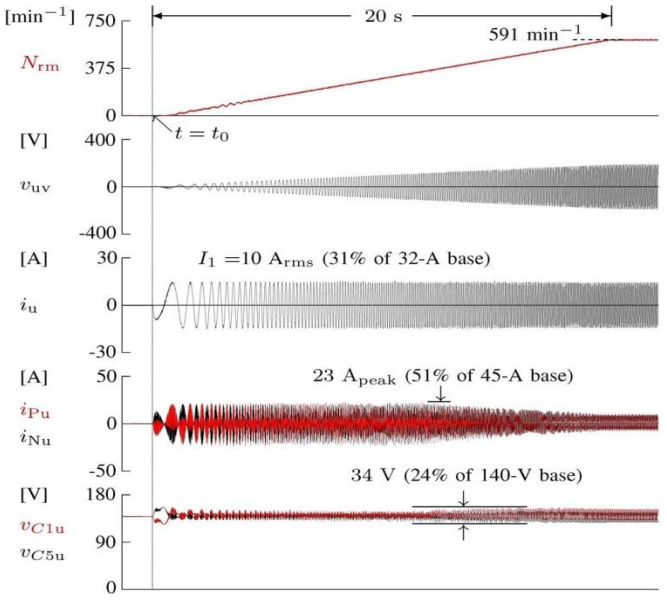

Fig 8: Experimental start-up waveforms when I = 10 A (31%) and T_L = 20%, where I_0 = 7.0 A (38%)

The peak-to-peak ac-voltage fluctuation of v_{C1u}^* and $vC5u$ was 34 V, which is 24% of 140 V. Fig. 9 shows the experimental start-up performance with TL = 20%. Here, I_1^* was set to 17A (53%), which is intended for comparisons with Fig. 8. The magnetizing current $I0$ estimated from Vuv reached 16.6A (90%). This current value of $I0$ = 16.6 A is the maximum current in this experimental condition because the over current protection of the arm currents works when $I0$ gets more than 16.6 A. The motor mechanical speed was increasing up to 597 min−1, where the slip frequency was fs = 0.10 Hz. The maximum amplitude of the arm currents was 46 A, which is 101% of 45 A. The peak-to-peak ac voltage fluctuation of $vC1u$ and $vC5u$ was 51 V, which are 36% of 140 V. The arm-current amplitude and the peak-to-peak ac voltage fluctuation increased by 50% and 12%, respectively, as compared to those in Fig. 8. These experimental results verified that the motor-speed control with the minimal stator current is effective in reductions of both arm-current amplitude and peak to- peak ac-voltage fluctuation.

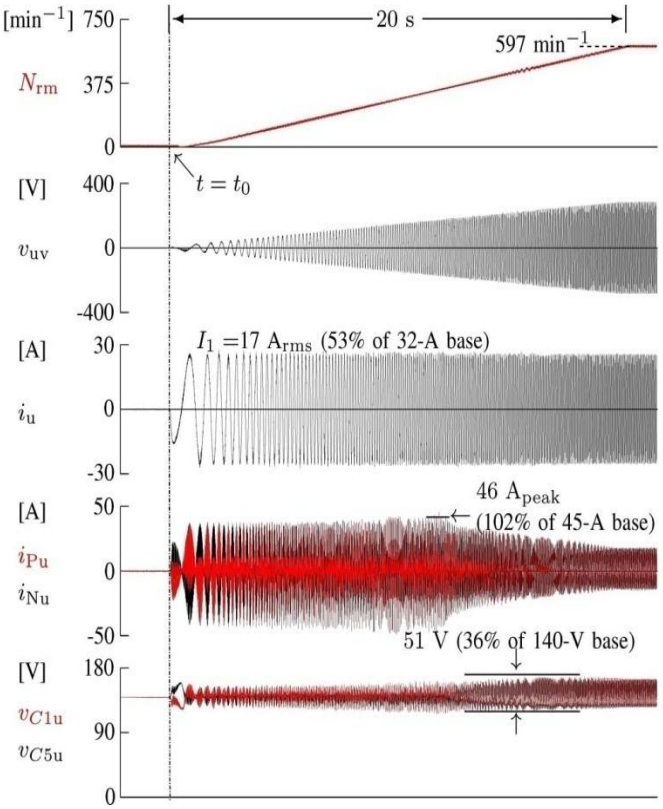

Fig 9: Experimental start-up waveforms when I_1^* = 17 A (53%) and T_L = 20%, where I_0 = 16.6 A (90%).

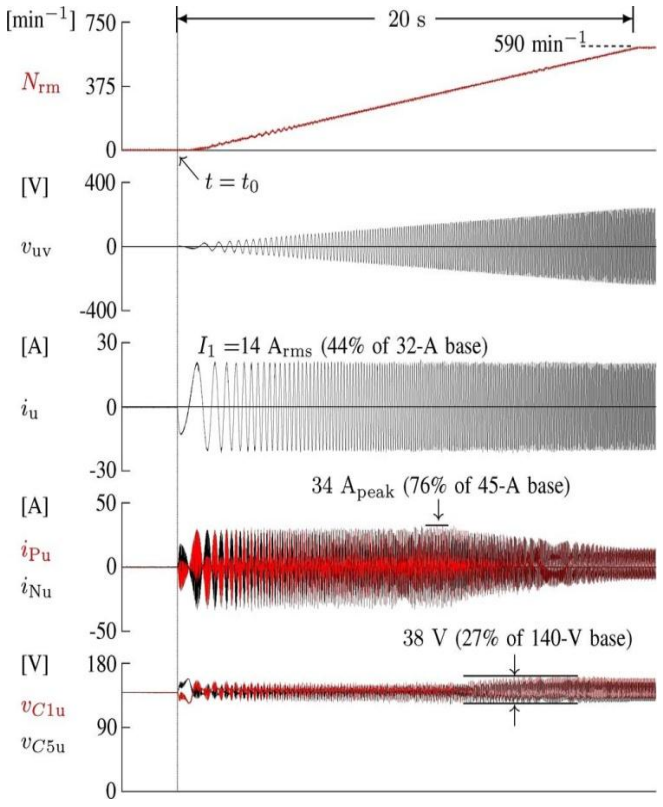

Fig 10: Experimental start-up waveforms when I = 14 A(44%), and T_L = 40%, where I_0 = 9.9 A (54%).

Fig. 10 shows the experimental start-up performance with T_L = 40%. Here, I_1^* was adjusted to 2 times of that when T_L = 20%, because I_1^* is proportional to a square root of torque according to (15). Hence, I_1^* was changed to 14A (= 2 10A, 44%). The magnetizing current I_0 reached 9.9A (= 14A$\sqrt{2}$, 54%). The motor mechanical speed was increasing up to 590 min^{-1}, where the slip frequency was f_s = 0.33 Hz. The maximum amplitude of the arm currents was 34A, which is 76% of 45A. The peak-to-peak ac-voltage fluctuation of v_{C1u} and v_{C5u} was 38 V, which is 27% of 140 V.

Fig. 11 shows the experimental start up performance with T_L = 60%. Here,I_1^* was set to 17A (=3×10A, 53%). The magnetizing current I_0 reached 12.0A (= 17A$\sqrt{2}$, 65%). The maximum amplitudes of the arm current and the peak-to- peak ac-voltage fluctuation were the same as those in Fig. 9, becauseI_1^* was set to the same value as Fig 9. The motor mechanical speed was decreasing to 588 min^{-1}, and the slip frequency was increasing to f_s = 0.4 Hz due to the increase of T_L. These experimental results show that the motor-speed control with the minimal stator current makes it possible to increase a start-up torque by a factor of three, without additional stress on arm currents and ac-voltage fluctuations, as compared to those in Fig. 9.

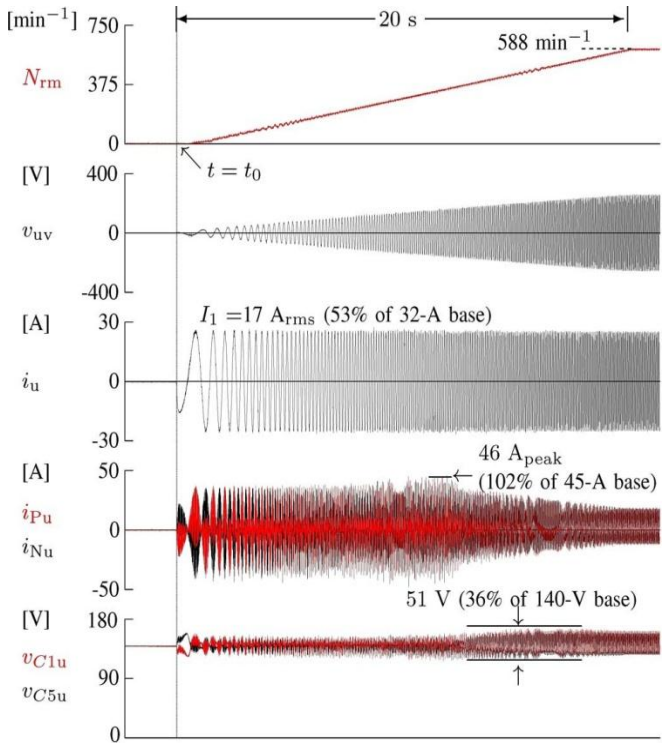

Fig 11: Experimental start-up waveforms when I = 17 A (53%), and T_L = 60%, where I_0 = 12.0 A (65%).

These experimental results show that the motor-speed control with the minimal stator current makes it possible to increase a start-up torque by a factor of three, without additional stress on arm currents and ac-voltage fluctuations, as compared to those in Fig. 9.

2.3 Steady-State Performance

Figs. 12–14 show experimental waveforms in steady states at different frequencies of operation. Here, I and T_L were set to I_1^* = 17 A (53%) and T_L = 60%, respectively

Fig. 12 shows those at f ∗ = 1 Hz. Here, the common-mode voltage with Vcom = 180 V and fcom = 50 Hz and the square- wave circulating currents were superimposed. The motor mechanical speed and the slip frequency were Nrm = 19 min−1 and fs = 0.38 Hz, respectively. The maximum amplitude of the arm currents was 38 A, which is 84% of 45 A. The peak-to-peak ac-voltage fluctuation of vC1u and vC5u was 34 V, which is 24% of 140 V.

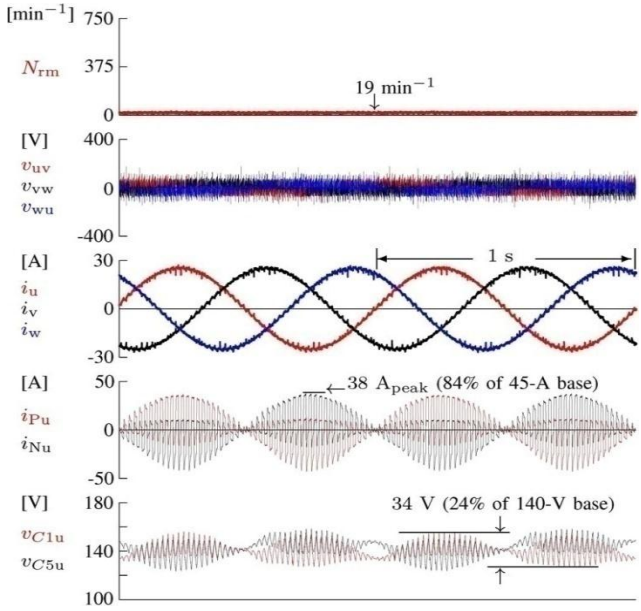

Fig 12: Experimental steady-state waveforms when I_1^* = 17 A (53%), f^* = 1 Hz, and T_L = 60%, where I_0 = 12.0 A (65%).

Fig. 14 shows those at f^* = 20 Hz. Here, V_{com} and the amplitude of the square-wave circulating currents were reduced to zero, because the ac-voltage fluctuation of each dc-capacitor voltage is not serious at this frequency. Although the peak value of the arm currents can be reduced to 19 A, which is 42% of 45 A, they contain the second-order frequency (40 Hz) component resulting from the control system [10]. The peak-to-peak ac-voltage fluctuation of v_{C1u} and v_{C5u} was 50 V, which is 36% of 140 V.

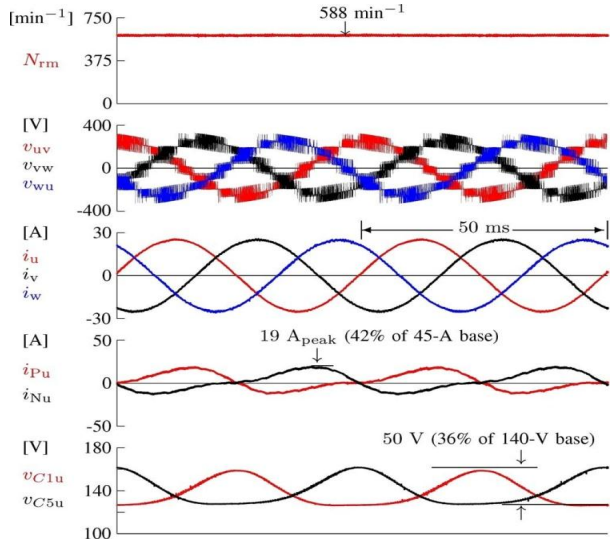

Fig 13: Experimental steady-state waveforms with I_1^* = 17 A (53%), f^* = 20 Hz, and T_L = 60%, where I_0 = 12.0 A (65%).

3.CONCLUSION

This paper has proposed a practical start-up method for a DSCC-driven induction motor with no speed sensor from steady state to middle speed. This start-up method is characterized by combining capacitor-voltage control and motor-speed control. The motor-speed control with the minimal stator current under a load torque is based on the combination of feedback control of the three-phase stator currents with feed forward control of their frequency and amplitude. The arm-current amplitudes and ac-voltage fluctuations across each of the dc capacitors can be minimizes to acceptable levels.

An experimental result obtained from a 400-V 15-kW down- scaled system has shown that the motor loaded with 60% can achieve a stable start up from steady state to a middle speed of N_{rm} = 588 min^{-1} without overvoltage and over current. The start-up torque has been increasing by a factor of three, without additional stress on both arm ac-voltage and currents fluctuations. This method is suitable particularly for adjustable-speed drives of large-capacity fans, blowers, and compressors for energy savings.

REFERENCES

[1] P. W. Hammond, "A new approach to enhance power quality for medium voltage ac drives," IEEE Trans. Ind. Appl., vol. 33, no. 1, pp. 202–208, Jan./Feb. 1997.

[2] R. Teodorescu, F. Blaabjerg, J. K. Pedersen, E. Cengelci, and P. N. Enjeti, "Multilevel inverter by cascading industrial VSI," IEEE Trans. Ind. Appl., vol. 49, no. 4, pp. 832–838, Jul./Aug. 2002.

[1] J. Rodriguez, S. Bernet, J. O. Bin Wu, and S. Pontt, "Multilevel voltage- source-converter topologies for industrial medium-voltage drives," IEEE Trans. Ind. Electron., vol. 54, no. 6, pp. 2930–2945, Dec. 2007.

[2] S. Malik and D. Kluge, "ACS 1000 world's first standard ac drive for medium-voltage applications," ABB Rev., no. 2, pp. 4–11, 1998.

[3] H. Akagi, "Classification, terminology, and application of the modular multilevel cascade converter (MMCC)," IEEE Trans. Power Electron., vol. 26, no. 11, pp. 3119–3130, Nov. 2011.

[4] A. Lesnicar and R. Marquardt, "An innovative modular multilevel con- verter topology suitable for a wide power range," in Conf. Rec. IEEE Bologna PowerTech, 2003, [CD-ROM].

[5] M. Hagiwara and H. Akagi, "Control and experiment of pulse-width- modulated modular multilevel converters," IEEE Trans. Power Electron., vol. 24, no. 7, pp. 1737–1746, Jul. 2009.

[6] M. Hiller, D. Krug, R. Sommer, and S. Rohner, "A new highly modular medium voltage converter topology for industrial drive applications," in Conf. Rec. EPE, 2009, pp. 1–10.

[7] S. Rohner, J. Weber, and S. Bernet, "Continuous model of modular multilevel converter with experimental verification," in Conf. Rec. IEEE- ECCE, 2011, pp. 4021–4028.

[8] M. Hagiwara, K. Nishimura, and H. Akagi, "A medium-voltage motor drive with a modular multilevel PWM inverter," IEEE Trans. Power Electron., vol. 25, no. 7, pp. 1786–1799, Jul. 2010.

[9] A. Antonopoulos, L. Angquist, S. Norrga, K. Llves, and H. P. Nee, "Mod- ular multilevel converter ac motor drives with constant torque from zero to nominal speed," in Conf. Rec. IEEE-ECCE, 2012, pp. 739–746.

[10] J. Kolb, F. Kammerer, and M. Braun, "Dimensioning and design of a modular multilevel converter for drive applications," in Conf. Rec. EPE, 2012, pp. LS1a-1.1-1–LS1a-1.1-8, [CD-ROM].

[11] A. J. Korn, M. Winkelnkemper, and P. Steimer, "Low output frequency operation of the modular multilevel converter," in Conf. Rec. IEEE-ECCE, 2010, pp. 3993–3997.

[12] M. Hagiwara, I. Hasegawa, and H. Akagi, "Startup and low-speed operation of an adjustable-speed motor driven by a modular multilevel cascade inverter (MMCI)," IEEE Trans. Ind. Appl., vol. 49, no. 4, pp. 1556–1565, Jul./Aug. 2013.

[13] J. Holtz, "Sensorless control of induction motor drives," Proc. IEEE, vol. 90, no. 8, pp. 1359–1394, Aug. 2002.

[14] R. J. Pottebaum, "Optimal characteristics of a variable-frequency centrifu- gal pump motor drive," IEEE Trans. Ind. Appl., vol. 20, no. 1, pp. 23–31, Jan. 1984.

[15] N. Hirotami, H. Akagi, I. Takahashi, and A. Nabae, "A new equivalent circuit of induction motor based on the total linkage flux of the secondary windings," Elect. Eng. Japan, vol. 103, no. 2, pp. 68–73, Mar./Apr. 1983.

[16] A. Munoz-Garcia, T. A. Lipo, and D. W. Novotny, "A new induction motor V/f control method capable of high-

performance regulation at low speeds," IEEE Trans. Ind. Appl., vol. 34, no. 4, pp. 813–821, Jul./Aug. 1998.

[17] H. Fujita, S. Tominaga, and H. Akagi, "Analysis and design of a dc voltage-controlled static var compensator using quad-series voltage- source inverters," IEEE Trans. Ind. Appl., vol. 32, no. 4, pp. 970–977, Jul./Aug. 1996.

[18] H. Peng, M. Hagiwara, and H. Akagi, "Modeling and analysis of switching-ripple voltage on the dc link between a diode rectifier and a modular multilevel cascade inverter (MMCI)," IEEE Trans. Power. Electron. vol. 28, no. 1, pp. 75–84, Jan. 2013.